"Soft Si": Effective Stiffness of Supported Crystalline Nanomembranes

Francesca Cavallo,* David S. Grierson, Kevin T. Turner, and Max G. Lagally

University of Wisconsin—Madison, Madison, Wisconsin 53706, United States

ABSTRACT We investigate the effective mechanical response of a layered system consisting of a thin crystalline sheet (nanomembrane) on a bulk substrate, with a high elastic mismatch (in the range of 5 to 9 orders of magnitude) between the stiff sheet and the compliant substrate. Using finite-element mechanics models and indentation experiments ranging from micro to nano, we show that the mismatch between the sheet and substrate elastic moduli, the length scale of deformation, and the sheet thickness all play a significant role in defining the effective stiffness of the layered system. For a wide range of indenter sizes, the mechanical response of the composite system is indistinguishable from that of the compliant substrate. In particular, at large indenter sizes, the mechanical response of the layered system is dominated by that of the compliant substrate. For decreasing indenter sizes, the effective stiffness of the layered structure reaches a finite value different from either the one expected for the compliant substrate or for a bulk crystal of the same material as the stiff top membrane.

KEYWORDS: layered materials · elastic mismatch · nanomembranes · effective compliance/stiffness · thinness · silicon · scale of deformation

Layered systems made of thin sheets of monocrystalline semiconductors bonded to flexible substrates have recently found application in extremely fast flexible electronics and novel optoelectronics.[1−7] The essential element in these advances is the monocrystalline freestanding semiconductor nanomembrane (FSNM).[8] FSNMs can have thicknesses ranging from a few nanometers to ∼1000 nm, with lateral areas from 0.03 to larger than 1 cm^2, and thus very large aspect ratios (width/thickness), in the range of 10^3 to more than 10^7. Modern advances in the release and transfer of such crystalline semiconductor sheets have enabled formation of layered substrates with extremely low bending stiffnesses, on which devices can be fabricated with performance comparable to that of devices formed on rigid substrates. Such devices can undergo various types of extreme mechanical deformation (*i.e.*, bending, stretching, and twisting) without degradation of their properties, and thus a variety of conformable, shaped, multidimensional electronics and optoelectronics have been realized.[1−7]

Multilayered systems used in bendable/stretchable electronics and optoelectronics are typically characterized by a large mismatch between the elastic moduli of an inherently stiff, but quite thin, top layer, such as Si, and a low-stiffness (*i.e.*, compliant) supporting substrate.[9,10] We will refer to such a materials system as an effectively compliant layered system (ECLS). In ECLSs, the low elastic modulus of the soft host dominates the mechanical response of the system, whereas the crystalline semiconductor sheet determines the charge transport, photonic, and surface properties. In this sphere, thinness leads to a prominence of surface effects and to the modification of many materials properties, such as electronic transport, phonon distributions, and, for sufficiently thin NMs, band structure and quantum properties.[11−13]

As the use of ECLSs in numerous applications is considered, a better description of their elastic response is needed. Despite the numerous demonstrations and applications of ECLSs, a quantitative understanding is lacking of how compliant an ECLS actually is. In this work, we investigate the mechanical response to indentation of an ECLS, consisting of a SiNM bonded to a low-modulus support, across multiple length scales. We present a combined theoretical and experimental study that demonstrates how nanomembrane/substrate elastic mismatch, nanomembrane thinness, and degree of deformation control the effective stiffness of the system. We establish the key relationships between properties and probe dimensions that define the load−deformation response and effective stiffness. We conclude by discussing the implications of our results as they relate to the integration of conventional semiconducting materials into biological environments.

* Address correspondence to fcavallo@wisc.edu.

Received for review February 3, 2011 and accepted May 23, 2011.

Published online June 06, 2011
10.1021/nn200461g

RESULTS AND DISCUSSION

Effectively compliant layered systems (ECLSs) used in high-performance device applications can be fabricated because intrinsically stiff materials (*e.g.*, Si and Ge), in the form of large-area, thin (5−100 nm) membranes, have exceptional compliance.[14,15] The stiffness of an elastic body is determined by the intrinsic elastic properties of the material (its elastic modulus) and by extrinsic factors, including the geometry of the body and the nature of applied loading. For instance, a planar elastic body of a given lateral size and a thickness, h, has axial and bending stiffnesses (the resistance to stretching/compression and to bending, respectively) that scale with $\sim h$ and $\sim h^3$, respectively.[16] These dependences explain why a material with the very high elastic modulus of Si (~148 GPa) appears effectively "soft" when made in ultrathin form: as h gets smaller, the ability of the material to deform elastically increases dramatically.

Prior investigations of the elastic response of ECLSs focused mainly on the macroscale, that is, on the distribution of stress (or strain) in the top coating of a thin-film composite resulting from bending with radii of curvature on the scale of a few millimeters.[1,6,9,10] For these studies, specially designed stages induce tensile and compressive strain in the top coating through axial and bending deformation of the compliant supporting substrate. Such methods yield an accurate estimation of the global mechanical response of multilayered systems but do not scale well into micro- and nanometer-sized regions. In contrast, several studies have recently reported on the integration of micro- and nanostructures (*e.g.*, quantum dots, nanoparticles, or biological cells) on supported/freestanding NMs and bulk compliant substrates.[11,17] The underlying idea in all of these studies is to use elastic interactions between the nanostructure and the supporting medium to tune the properties of their constitutive materials. To quantify such approaches requires accurate modeling of local deformation behavior and the impact of contact loading on the supporting medium and associated measurements of the system response to loading.

We have used a finite-element model (FEM) of a SiNM supported on a compliant substrate to predict the NM/substrate indentation response to various loading conditions and have performed corresponding experiments to measure the response. Indentation methods allow measuring the response of a materials system for varying loads, contact sizes from the micro- to the nanoscale, and indentation depths and are therefore a powerful way to investigate the mechanical response of homogeneous elastic bodies and of both supported and unsupported thin films.[18−27] Indentation has been extensively used to investigate layered systems, including both elastically homogeneous and elastically mismatched materials.[18−33] The majority of these previous studies was motivated by the desire to characterize the intrinsic elastic properties and failure mechanisms of supported thin films or coatings and therefore kept the elastic mismatch small, typically less than 2 orders of magnitude. In these studies, the influence of the substrate on the mechanical response is generally reported as a nuisance, and methods have been presented to correct for its effect on measurements.[18−28]

In contrast, we focus on the effective mechanical response of a layered system with a mismatch in the elastic moduli between the film and substrate ranging from 5 to 9 orders of magnitude. Our focus is to quantify the effective indentation response of ECLSs and therefore differs substantially from previous investigations aimed at extracting the true mechanical properties of a film that is of necessity supported on a substrate. We explore cases where the mechanical properties of the supporting substrate are selected to create effectively low-stiffness materials. Furthermore, in contrast to prior nanoindentation studies, the induced deformation in our ECLS is purely elastic.

We first determine the response to indenting a Si-based ECLS with a rigid flat-ended cylindrical punch. To analyze the indentation of the SiNM/substrate systems and the bulk substrates, we use an axisymmetric finite-element model. The model was developed and solved using the commercial finite-element software ABAQUS 6.3-1 (HKS, Rhode Island). The indenter is modeled as a rigid body with a flat-ended cylindrical shape of variable radius, a, in the range of 5 nm to 25.6 μm. The SiNM and substrate are assumed to be isotropic and linearly elastic, with Young's modulus E_{NM} = 148 GPa and Poisson's ratio ν_{NM} = 0.18, which are the average in-plane values for a (100) orientation. The elastic modulus of the substrates used in our finite-element analysis (FEA) is varied between 1 kPa and 1 MPa, in order to span the range of moduli encountered in widely available soft materials, such as polyacrylamide gels (PAAG) and polydimethylsiloxane (PDMS). The thickness of the substrates is 1 mm, and the materials systems are modeled as cylinders with a radius of 10 mm, fully constrained in all three directions at the base of the substrates and unconstrained at the periphery. The constraints enforced on the base of the model mimic our experimental condition, in which the specimen is effectively adhered to a metal holder. The large radius (*i.e.*, 10 mm) of the model, which was chosen through a convergence study, eliminates any sensitivity of the indentation response to the overall size of the substrate and the presence or lack of constraint forces along the periphery of the substrate.

The model is meshed with eight-node axisymmetric elements, with the mesh highly refined in the region below the indenter. The SiNMs are assumed to be perfectly bonded to the substrates. Two bounding cases, no friction and infinite friction, are examined

for the contact between the indenter and the NM surface. Displacements are applied to the indenter, and the reaction forces are recorded as a function of indenter displacement. The effective stiffness is defined as the slope of the calculated force–displacement response.

Figure 1a,b shows results corresponding to a SiNM bonded to two different substrates, A and B (subA and subB), with Young's moduli of E_{subA} = 10 kPa and E_{subB} = 1 MPa, and Poisson's ratios $\nu_{subA} = \nu_{subB}$ = 0.499. A frictionless contact between the indenter and the SiNM surface is assumed. Including an infinite friction at the punch/SiNM interface does not yield significantly different results. In Figure 1a, stiffness is plotted *versus* contact radius for the NM/sub A and NM/sub B systems, both bulk compliant substrates by themselves, and bulk Si by itself. In the bulk cases, a linear relationship between stiffness and contact radius is observed. This result is supported by a well-defined analytical solution for the stiffness, k, for indentation of a homogeneous, isotropic, linear-elastic infinite half-space by a frictionless, rigid, flat punch

$$k = \frac{2aE}{(1 - \nu^2)} \quad (1)$$

where E and ν are the Young's modulus and Poisson's ratio of the material, respectively, and a is the radius of the flat punch.[34]

The effective stiffness of the NM/substrate system follows a trend as a function of contact radius that differs from that described by eq 1. At large contact radii, the effective stiffness of the SiNM/substrate system follows that of the thick, very compliant substrate. For example, for substrate B, at a contact radius of ~25 μm, the effective stiffness of the NM/sub B is lower by a factor of ~80 000 relative to that of bulk Si. For a NM on a substrate with an even lower elastic modulus, such as substrate A, the reduction in stiffness of the layered system relative to bulk Si is even more dramatic, ~10^7 at a contact radius of 25 μm. For sufficiently small contact radii, the stiffness of the layered system becomes independent of the size of the contact but is still much lower than that of bulk Si. So, for example, with a 5 nm contact radius, the model for the 25 nm SiNM on substrate B exhibits a stiffness that is approximately 200 times lower than the value expected for bulk Si. On the less stiff substrate A, with a 5 nm indenter radius, the SiNM exhibits a stiffness of the order of 10^4 less than bulk Si. The conclusions of Figure 1a are in contrast to prior results obtained for layered materials with a low elastic mismatch, which showed that indenters with radius comparable to the top-layer thickness yield the mechanical response of the coating. Here, even with a small contact radius, the effective stiffnesses are strongly influenced by the substrate, even though the indenter radius is even smaller than the top-film thickness.

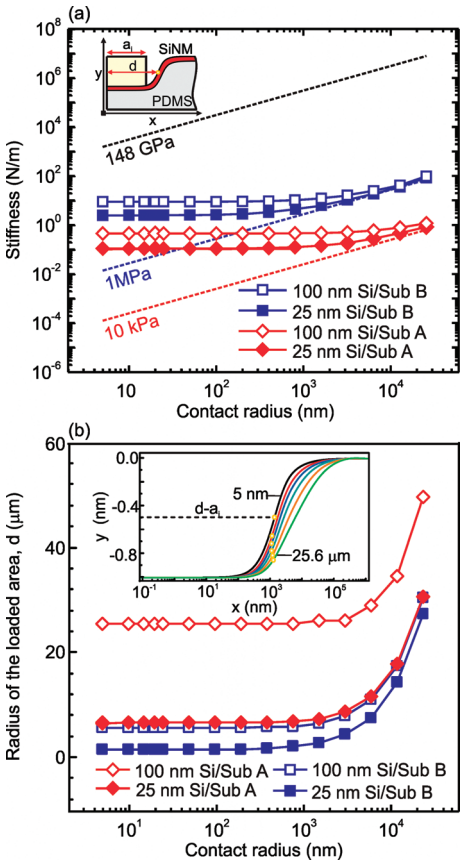

Figure 1. Stiffness of layered and bulk systems under normal loading by a flat punch. (a) Normal stiffness *vs* contact radius as determined by FEA for a rigid, cylindrical flat punch indenting into three bulk materials with elastic moduli of 10 kPa (substrate A, red dashed line corresponding roughly to PAAG), 1 MPa (substrate B, blue dashed line, corresponding roughly to PDMS), 148 GPa (black dashed line, corresponding to bulk Si); 25 and 100 nm SiNMs on substrate A (red solid diamonds and red open diamonds, respectively); and 25 and 100 nm SiNMs on substrate B (blue solid squares and blue open squares, respectively). The contact radius, *a*, is the radius of the cylindrical indenter, and the SiNM is assumed to be perfectly bonded to the PDMS substrate. The elastic moduli and Poisson's ratios used in the FEA were E_{NM} = 148 GPa and ν_{NM} = 0.18; E_{subA} = 10 kPa and ν_{subA} = 0.499; and E_{subB} = 1 MPa and ν_{subB} = 0.499. The inset illustrates schematically a typical profile of an indented-NM/substrate system. (b) Distance, *d*, between the center of the flat punch and the inflection point of the deformed SiNM profile plotted *versus* contact radius, *a*. The inset displays the profiles of a deformed 25 nm SiNM/sub B system, shifted by the flat punch radius *a*, for different values of *a*. Open circles mark the positions of the inflection points.

We discuss the trends shown in Figure 1a in terms of a simple physical model. To an indenter applying a normal load to a Si-based ECLS, the SiNM and the soft substrate appear as two linear springs in series, with spring constants k_{NM} and k_{Sub}. Hence the effective stiffness of the layered system can be written as $k = [k_{Sub}^{-1} + k_{NM}^{-1}]^{-1}$. Owing to its low-stiffness relative to the SiNM ($k_{Sub} \ll k_{NM}$), the substrate takes up the majority of the elastic compression generated by indentation loading. As a result, the effective stiffness

of the ECLS at a given indenter size is defined by the volume of material in the soft substrate that is deformed and hence contributes to the mechanical response. In turn, the extent of the loaded area in the soft substrate is determined by the elastic response of the supported NM to indentation loading.

In particular, at small contact radii (such that the normalized contact radius a/h is lower than ~20 for NMs/sub A and lower than ~4 for NMs/sub B, in Figure 1a), the intrinsic stiffness of the NM determines the volume of material in the soft substrate that is deformed and hence contributes to the mechanical response; that is, the high stiffness of the NM allows only a slow increase of the contact area and in turn of the area of the substrate contributing to the mechanical response. In this limit, therefore, an increase in the size of the contact results in a negligible change in the deformation behavior of the NM/substrate system. At larger indenter radii, the deformation behavior of the supported NM is progressively more affected by the mechanical properties of the supported substrate, which leads to a more rapid increase of the contact area. In the extreme case of $a \gg h$, the volume of material in the soft substrate that contributes to the mechanical response is determined completely by the indenter size and the mechanical response of the substrate, thus the effective stiffness of the ECLS approaches that of the supporting soft substrate. The transition between these regimes of a-independent and a-dependent system stiffness occurs at a critical ratio, a_c/h, that is a function of the stiffness mismatch between the Si film and the substrate. A more detailed discussion of this aspect follows later in the text.

We investigate the deformation profile of the surface of the NM/substrate system by indenters of varying radii. The aim is to correlate the intrinsic deformation behavior of the layered system with its effective stiffness. Figure 1b shows results, corresponding to those in Figure 1a, of the distance, d, of the inflection point of the curved-NM profile from the center of the indenter. The distance d characterizes the extent of lateral deformation of the NM/substrate system and directly correlates with changes in the system stiffness. The inset in Figure 1b shows the profiles of curved NMs at various indenter radii, with the position of the inflection point also marked. The position of the inflection point of the deformed-NM profile relative to the indenter's center is a measure of the volume of material in the substrate that is elastically deformed by the applied loading. As our qualitative discussion above suggests, the coordinates of the inflection points remain nearly constant for a range of small indenter sizes, and the extent of the loaded region also stays constant. As the indenter size is increased beyond a certain point, the coordinates of the inflection points vary, demonstrating a change, particularly an increase, in the size of the loaded region, and suggesting that the effective

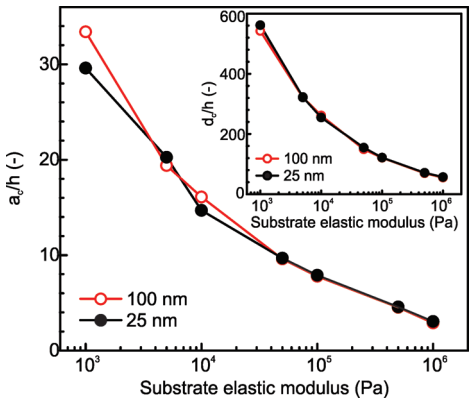

Figure 2. Normalized critical contact radius, a_c/h, defining the transition between radius-independent and radius-dependent stiffness plotted as a function of the elastic modulus of the supporting substrate. The inset shows the corresponding normalized distance d_c/h of the inflection point of the deformed SiNM from the axis of the cylindrical indenter.

stiffness increases as well. The expected correlation between the position of the inflection points and the effective stiffness can be seen by comparing the trends in Figure 1b with those in Figure 1a.

As Figure 1a shows, the transition between the a-independent and a-dependent system stiffness occurs at different a_c/h ratios for SiNMs on substrates A and B. Figure 2 elucidates this effect by summarizing the a_c/h ratios as a function of the elastic modulus of the supporting substrate. Below the critical contact radius, a_c, a stiffness change of less than 5% is observed when varying a. This critical contact radius defines the upper limit of the a-independent stiffness regime. Corresponding d_c/h values (*i.e.*, the normalized d value measured at $a = a_c$) are plotted in the inset. Figure 2 shows that low-modulus substrates yield higher values for both a_c/h and d_c/h. The amount of NM axial and bending strain (*i.e.*, stretching and curvature) that can be maintained by a supporting substrate decreases with decreasing substrate modulus, hence the increase in d_c with decreasing E_{sub}.

The effective stiffnesses of 25 nm thick SiNM/PDMS and bulk PDMS substrates were investigated experimentally on a large lateral scale by indenting with a flat punch of radius 225 μm. At this indenter size, the effective stiffness of the SiNM/PDMS system is indistinguishable, within experimental error, from the stiffness of bulk PDMS, at a value of $\sim(1.02 \times 10^3) \pm 20$ N/m. This value agrees with that calculated for bulk PDMS using eq 1, with $a = 225$ μm, $E = 1.7$ MPa, and $\nu = 0.45$. As predicted by FEA and shown in Figure 1a, at this indenter radius, the SiNM/PDMS system is effectively as compliant as bare PDMS.

To probe effective stiffnesses for small indenter sizes, we use an atomic force microscope (AFM).[35] AFM probes with parabola-shaped tips were used in this investigation because flat-ended cylindrical AFM tips with appropriate tilt compensation are not

available. To simulate the deformation that would occur by AFM-based nanoindentation, we use FEA to model a parabolic tip indenting into a SiNM/PDMS system. The mechanical properties and shape of the indenter were selected to resemble the ultrananocrystalline diamond (UNCD) AFM probe tips that we used (E_{tip} = 850 GPa, ν_{tip} = 0.1), and the elastic properties of the PDMS substrate were matched to those measured experimentally, namely, E_{PDMS} = 1.5 ± 0.07 MPa and ν_{PDMS} = 0.45 ± 0.02. The simulations provide insight into the influence of the quality of the film–substrate interface and the concentrated stress distribution on the deformation behavior, and guide the AFM experimentation. Figure 3 shows the deformation response to the force of a parabolic tip indenting into several SiNM/PDMS systems, with membrane thicknesses ranging from 25 to 220 nm. Both perfectly bonded (dashed-dotted lines) and unbonded (solid lines) NMs on PDMS were modeled. The mechanical response of the system is linear in all cases, with an increase in NM thickness leading to an increase in slope (*i.e.*, increase in effective stiffness). A linear force–displacement ($F-\delta$) response is not expected for a spherical contact on a semi-infinite half-space.[34] When a sphere is pressed on an elastic material, the contact area (as well as the load) undergoes a typically $\sim\delta^{3/2}$ Hertzian response, a nonlinear increase.[34] For soft materials with a high-modulus skin (*e.g.*, SiNM/PDMS), however, an increase in displacement results in a negligible amount of local deformation at the tip–film interface. Most of the compression (>90% for 25 and 100 nm thick SiNMs) is due to indentation occurring in the PDMS substrate. The contact area at the NM–indenter interfaces remains nearly constant with displacement, producing the observed linear response.

Force–displacement responses calculated by FEA and plotted in Figure 3 show that an insignificantly lower slope (lower stiffness) is measured for the force–displacement curves of SiNM/PDMS with frictionless interfaces compared to SiNMs perfectly bonded to the compliant PDMS support. We conclude that possible slipping of the NM on the host substrate has a negligible influence on the effective normal stiffness of the NM/PDMS system.

Figure 4 compares relevant AFM indentation measurements to the FEA $F-\delta$ response of bulk PDMS and of a 25 nm SiNM/PDMS layered system. The $F-\delta$ response for bulk PDMS is nonlinear, while that of the 25 nm SiNM/PDMS is linear (see Figure 3), with the PDMS exhibiting a much lower stiffness than the composite for a small indenter, as expected from Figure 1a. The curve measured for the bulk PDMS corresponds to a typical $\sim\delta^{3/2}$ Hertzian response of a sphere indenting on a homogeneous elastic half-space. We expect that in the limit of a vanishingly thin SiNM the ECLS recovers the Hertzian contact response.

Figure 5 shows effective stiffness values obtained by AFM nanoindentation (7–15 nm radius indenter) and

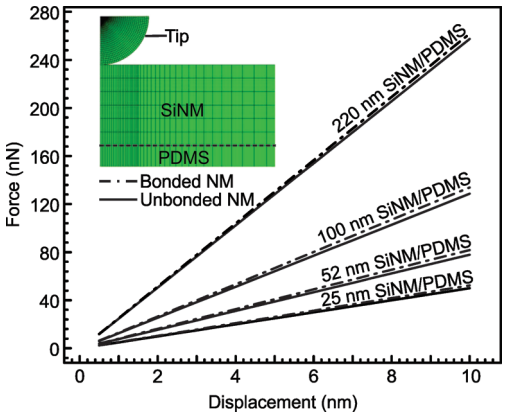

Figure 3. Indentation of SiNM/PDMS systems under AFM-type loading. Force *versus* displacement responses from FEA of a spherical tip (E_{tip} = 800 GPa, ν_{tip} = 0.1) indenting on a SiNM/PDMS system with SiNMs having thicknesses in the range of 25 to 220 nm. The mechanical properties and shape of the indenter were selected to represent the UNCD AFM tips used during experimentation. Both perfectly bonded (dashed-dotted lines) and unbonded (solid lines) NMs on PDMS were modeled to assess the sensitivity to bonding at the interface. The mechanical response of the material was found to be linear in all cases, with an increase in NM thickness leading to an increase in effective stiffness (slope of force–displacement curves).

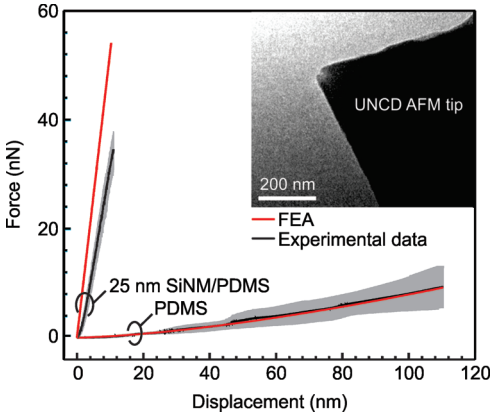

Figure 4. Comparison of the force–displacement response obtained by FEA and AFM nanoindentation using a UNCD parabolic tip with a radius in the range of 7–15 nm indenting into 25 nm SiNM/PDMS and bulk PDMS. The responses to both indentation loading and unloading coincide, showing that all indentation is in the elastic regime. The force–displacement curves displayed here correspond to the average response acquired during 70 different indentation tests on a 25 nm Si NM/PDMS and bulk PDMS, with the area shaded in gray representing the standard deviation of these tests. The inset is a TEM image of one of the UNCD tips used in the nanoindentation experiments.

FEA for SiNM/PDMS systems for various SiNM thicknesses, ranging from 25 to 220 nm. FEA results for both perfectly bonded and unbonded NMs are shown. The experiments confirm that SiNM/PDMS systems are significantly less stiff (at least 2 orders of magnitude) than bulk Si for the same indenter size, as first shown in Figure 1a. The trend of increasing effective stiffness with increasing NM thickness is observed in both

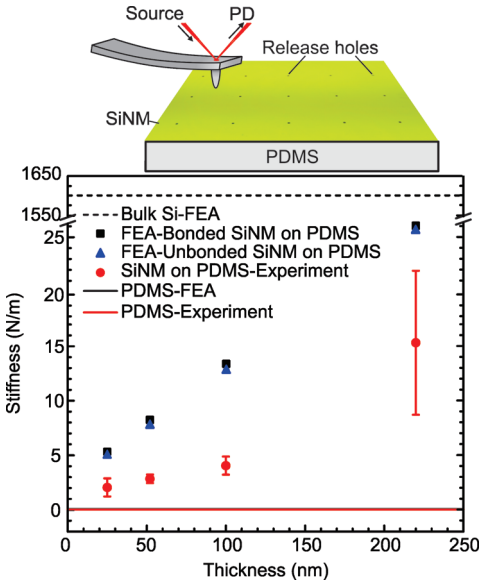

Figure 5. Stiffness *versus* SiNM thickness calculated by FEA (black solid squares and blue solid triangles) and measured by AFM-based nanoindentation (red solid circles) for the SiNM/PDMS system. FEA results for bulk Si (black dashed line) and FEA and experimental results for bulk PDMS (red and black solid lines) are included for reference. The black and red solid lines coincide. A spherical tip with a radius of 10 nm was used in the FEA. Tips with radii in the range of 7−15 nm were used in the nanoindentation experiments. The indentation process of a SiNM/PDMS sample is sketched in the top panel.

experimental results and FEA. The measured values of effective stiffness are, however, even lower than those expected from the FEA results for all NM thicknesses. Possible thickness variations in the SiNMs, the nonconformity of the SiNM to the PDMS resulting from a long-range roughness of the PDMS substrates, and voids at the SiNM/PDMS interface may contribute to this discrepancy.

CONCLUSIONS

We have demonstrated that the effective stiffness of a single-crystal (high-stiffness) semiconductor sheet on a low-modulus substrate, with a high mismatch in their elastic moduli (>10^5), is defined by the elastic moduli of the constitutive materials and the thickness of the sheet, as well as by the extent of the loaded area. We establish the key relationships between properties and probe dimensions (*i.e.*, indenter radii) that define the load−deformation response and effective stiffness. Specifically, we demonstrate how the scale of deformation (*i.e.*, the extent of the contact area in the indentation) of SiNM/compliant substrate systems defines the elastic response to an applied load. Simulation and indentation tests performed with indenters of various sizes show that the response of SiNMs on compliant substrates approaches that of the bare substrate when the indenter radius is larger than tens of micrometers, with the values somewhat influenced by the compliancy of the substrate.

The ability to transfer large-area nanomembranes of stiff semiconductors and other materials to compliant substrates can be used to create layered composites with an effective stiffness that can be tuned over a wide range. An appropriate selection of the NM element allows fabrication of supported highly compliant structures with the excellent electronic, optical, and magnetic properties of the corresponding bulk functional material.

A significant implication of our results concerns integration of engineered devices in biological environments. Several studies have shown that cells are able to sense and actively respond to their mechanical environment.[17,36] The compliance of the cellular environment can affect the adhesive interactions, the internal cytoskeletal structure, the migration behavior, and the overall state of the cell. To understand cell−substrate interactions requires careful consideration of the stiffness of materials at the interface between the devices and cells. The elastic modulus of a typical natural cellular environment is on the order 1−100 kPa, while conventional device constitutive materials (*e.g.*, metals, dielectrics, and inorganic semiconductors) have elastic moduli in the range of 10−200 GPa. This large difference in elastic modulus makes it a significant challenge to integrate semiconductor and photonic devices with biological cells without altering the cell state. The typical contact radius of a biological cell lies in the 1−100 μm range during the various stages of its growth. Figure 1a shows that for such large contact radii the mechanical response of thin semiconductor films on compliant hosts is determined by that of the host. This result suggests that an appropriate selection of the compliant host allows us to create inorganic devices with stiffness matching the one of a typical cellular environment.

METHODS

Sample Preparation. SiNM/PDMS systems are fabricated with SiNMs having lateral sizes ranging from 200 × 200 μm^2 to 4 × 4 mm^2 and thicknesses from 25 to 220 nm. SiNMs are made from Si-on-insulator (SOI) wafers, consisting of a 220 nm thick Si template, a 3 μm thick buried oxide (BOX) layer, and a bulk Si handle wafer. Thermally oxidizing the starting template and etching the grown oxide produces thinner SiNMs. Selectively etching the BOX [using HF (49 vol %)] makes the SiNMs freestanding. In some cases, release holes[8] are patterned into the Si template to enhance access of the etchant to the BOX. Photolithography and reactive ion etching in a SF_6/O_2 plasma are used for this purpose. After complete removal of the BOX, SiNMs are rinsed in DI water and transferred onto a PDMS substrate.

The PDMS substrates are prepared by casting a liquid PDMS mixture (10:1 weight ratio of silicone elastomer to curing agent,

Sylgard 184, Dow Corning) onto RCA-cleaned Si wafers and curing on a hot plate at 85 °C for 4 h. The thickness of the PDMS substrates is approximately 2 mm. After peeling it off the Si wafer, the PDMS is ultrasonicated for 20 min in DI water, dried and then exposed to an oxygen plasma for 30 s at a power of 50 W. Oxygen plasma treatment improves adhesion by removing surface contaminants and introducing atomically roughened bonding surfaces and reactive chemical groups.[37] The released SiNMs are immediately transferred onto the PDMS substrates after oxygen plasma treatment.

Nanoindentation Experiments. Nanoindentation is performed with a MultiMode atomic force microscope (AFM) (Bruker/Digital Instruments) in contact mode using ultrananocrystalline diamond (UNCD) AFM probes (Advanced Diamond Technologies, Romeoville, IL). The spring constants of the AFM cantilevers are calibrated by measuring their force response against calibrated reference levers (Advanced Diamond Technologies, Romeoville, IL). By pushing the cantilever of unknown spring constant against a reference lever of known spring constant and determining the slope of the linear force *versus* deformation response, the spring constant of the unknown lever can be calculated by considering the two levers as two springs in series. A JEOL 100CX TEM was used to examine the AFM tips before and after the indentation measurements to ensure that the tips were neither damaged nor contaminated during the indentation tests. The tip shape is determined quantitatively using the blind reconstruction method[38] by acquiring AFM images of UNCD surfaces and using the commercial SPIP (Scanning Probe Image Processor) software package to execute the blind-reconstruction algorithm. The radius of the tip is obtained from a parabolic fit to the 3D tip shape generated by the SPIP software.

Each data point in Figure 5 corresponds to an average of 70 measurements, with the error bars representing the standard deviation. Nanoindentation was performed at three different locations on each specimen, spaced at least 400 μm apart. The stiffness of the specimen was determined by finding the slope of the force *versus* deformation response over the applied load range of ~0−10 nN. Both AFM inspection of the indented areas and agreement (within the limit of the experimental error) between results of repeated indentation tests at the same location confirm that all of the measurements were performed in the elastic regime.

Characterization of the PDMS Substrates. The elastic modulus and Poisson's ratio used for the PDMS substrates in the FEA analysis are measured using tensile tests. Four gold markers, arranged in a rectangular pattern, were deposited on a PDMS specimen with a thickness of ~2 mm and lateral dimensions of 7.9 × 3.4 mm^2. The gold markers are fabricated by sputter deposition through a shadow mask. The specimen was tested in uniaxial tension at a loading rate of 2 mm/min up to a maximum strain of approximately 5% using an MTS testing machine (Eden Prairie, MN). A Sony HDR-CX500 camcorder (Sony Electronics Inc.), with a resolution of 12.0 megapixels and frame-capture rate of 30 fps, is used to record the positions of the Au marks during testing, and a custom Matlab script (Mathworks Inc.) is used to process the images in order to track the positions of the marks.

A Poisson ratio of 0.45 ± 0.02 was measured as the ratio of lateral and normal strain $\nu = \varepsilon_l/\varepsilon_n$. Normal and lateral strain describe relative deformation in the directions parallel and perpendicular to the applied load, respectively. Both strains are measured as relative changes in the original distances of the Au marks caused by the applied load. An elastic modulus of 1.5 ± 0.07 MPa was obtained as the ratio of the applied stress and measured strain in the direction of applied load.

Acknowledgment. This research was supported primarily by AFOSR-MURI, Grant No. FA9550-08-1-0337. Experiments were partially supported by NSF, Grant No. DMR 0906930. Facilities support was provided by NSF-MRSEC, Grant No. DMR-0520527. We thank M. Huang and M. Wald for experimental help.

REFERENCES AND NOTES

1. Menard, E.; Nuzzo, R. G.; Rogers, J. A. Bendable Single-Crystal Silicon Thin-Film Transistors Formed by Printing on Plastic Substrates. *Appl. Phys. Lett.* **2005**, *86*, 093507(1−3).
2. Yuan, H. C.; Ma, Z. Q.; Roberts, M. M.; Savage, D. E.; Lagally, M. G. High-Speed Strained-Single-Crystal Silicon Thin-Film Transistors on Flexible Polymers. *J. Appl. Phys.* **2006**, *100*, 013708(1−3).
3. Ahn, J.-H.; Kim, H.-S.; Menard, E.; Lee, K. J.; Zhu, Z.; Kim, D.-H.; Nuzzo, R. G.; Rogers, J. A.; Amlani, I.; Kushner, V.; *et al.* Bendable Integrated Circuits on Plastic Substrates by Use of Printed Ribbons of Single-Crystalline Silicon. *Appl. Phys. Lett.* **2007**, *90*, 213501(1−3).
4. Kim, D.-H.; Song, J.; Choi, W. M.; Kim, H.-S.; Kim, R.-H.; Liu, Z.; Huang, Y. Y.; Hwang, K. C.; Zhang, Y.-W.; Rogers, J. A. Materials and Non-coplanar Mesh Designs for Integrated Circuits with Linear Elastic Responses to Extreme Mechanical Deformations. *Proc. Natl. Acad. Sci. U.S.A.* **2008**, *105*, 18675–18680.
5. Yuan, H. C.; Shin, J. Y.; Qin, G. X.; Sun, L.; Bhattacharya, P.; Celler, G. K.; Lagally, M. G.; Ma, Z. Q. Flexible Photodetectors on Plastic Substrates by Use of Printing Transferred Single-Crystal Germanium Membranes. *Appl. Phys. Lett.* **2009**, *94*, 013102(1−3).
6. Ko, H.; Takei, K.; Kapadia, R.; Chuang, S.; Fang, H.; Leu, P. W.; Ganapathi, K.; Plis, E.; Kim, H.; Chen, S.-Y.; *et al.* Ultrathin Compound Semiconductor on Insulator Layers for High-Performance Nanoscale Transistors. *Nature* **2010**, *468*, 286–289.
7. Sun, L.; Qin, G; Seo, J.-H.; Celler, G. K.; Zhou, W.; Ma, Z. 12-GHz Thin-Film Transistors on Transferrable Silicon Nanomembranes for High-Performance Flexible Electronics. *Small* **2010**, *6*, 2553–2557.
8. Roberts, M. M; Klein, L. J.; Savage, D. E.; Slinker, K. A.; Friesen, M.; Celler, G. K.; Eriksson, M. A.; Lagally, M. G. Elastically Relaxed Free-Standing Strained-Si Nanomembranes. *Nat. Mater.* **2006**, *5*, 388–393.
9. Ko, H. C.; Shin, G.; Wang, S.; Stoykovich, M. P.; Lee, J. W.; Kim, D.-H.; Ha, J. S.; Huang, Y.; Hwang, K.-C.; Rogers, J. A. Curvilinear Electronics Formed Using Silicon Membrane Circuits and Elastomeric Transfer Elements. *Small* **2010**, *5*, 2703–2709.
10. Wang, S.; Xiao, J.; Song, J.; Ko, H. C.; Hwang, K. C.; Huang, Y.; Rogers, J. A. Mechanics of Curvilinear Electronics. *Soft Matter* **2010**, *6*, 5757–5763.
11. Huang, M.; Ritz, C. S.; Novakovic, B.; Yu, D.; Zhang, Y.; Savage, D. E.; Flack, F. S.; Evans, P. G.; Knezevic, I.; Liu, F.; Lagally, M. G. Mechano-electronic Superlattices in Silicon Nanoribbons. *ACS Nano* **2009**, *3*, 721–727.
12. Scott, S. A.; Peng, W.; Kiefer, A. M.; Jiang, H.; Knezevic, I.; Savage, D. E.; Eriksson, M. A.; Lagally, M. G. Influence of Surface Chemical Modification on Charge Transport Properties in Ultrathin Silicon Membranes. *ACS Nano* **2009**, *3*, 1683–1692.
13. Chen, F.; Ramayya, E. B.; Euaruksakul, C.; Himpsel, F. J.; Celler, G. K.; Ding, B.; Knezevic, I.; Lagally, M. G. Quantum Confinement, Surface Roughness, and the Conduction Band Structure of Ultrathin Silicon Membranes. *ACS Nano* **2010**, *4*, 2466–2472.
14. He, J.; Kunitake, T. Are Ceramic Nanofilms a Soft Matter? *Soft Matter* **2006**, *2*, 119–125.
15. Cavallo, F.; Lagally, M. G. Semiconductors Turn Soft: Inorganic Nanomembranes. *Soft Matter* **2010**, *6*, 439–455.
16. Audoly, B.; Pomeau, Y. *Elasticity and Geometry: From Hair Curls to the Non-Linear Response of Shells*; Oxford University Press: New York, 2010.
17. Discher, D. E.; Janmey, P.; Wang, Y. Tissue Cells Feel and Respond to the Stiffness of Their Substrate. *Science* **2005**, *310*, 1139–1143.
18. Burnett, P. J.; Rickerby, D. S. The Mechanical Properties of Wear-Resistant Coatings: I: Modelling of Hardness Behaviour. *Thin Solid Films* **1987**, *148*, 41–50.
19. Bolshakov, A.; Pharr, G. M. Influence of Pile-up on the Measurements of Mechanical Properties by Load and Depth Sensing Indentation Techniques. *J. Mater. Res.* **1998**, *13*, 1049–1058.
20. Yoffe, E. H. The Elastic Compliance of a Film on a Substrate. *Phil. Mag. Lett.* **1998**, *77*, 69–78.
21. Saha, R.; Nix, D. Effects of the Substrate on the Determination of Thin Film Mechanical Properties by Nanoindentation. *Acta Mater.* **2002**, *50*, 23–28.

22. Zheng, Z. W.; Sridhar, I. Spherical Indentation of an Elastic Thin Film on an Elastic–Ideally Plastic Substrate. *Mater. Sci. Eng., A* **2006**, *423*, 64–69.
23. McGuiggan, P. M.; Wallace, J. S.; Smith, D. T.; Sridhar, I.; Zheng, Z. W.; Johnson, K. L. Contact Mechanics of Layered Elastic Materials: Experiment and Theory. *J. Phys. D: Appl. Phys.* **2007**, *40*, 5984–5994.
24. Buršikova, V.; Sládek, P.; St'ahel, P.; Buršik, J. Mechanical Properties of Thin Silicon Films Deposited on Glass and Plastic Substrates Studied by Depth Sensing Indentation Technique. *J. Non-Cryst. Solids* **2006**, *352*, 1242–1245.
25. Nguyen, T. D.; Yeager, J. D.; Bahr, D. F.; Adams, D. P.; Moody, N. R. Nanoindentation of Compliant Substrate Systems: Effects of Geometry and Compliance. *J. Eng. Mater. Technol.* **2010**, *132*, 021001(1–7).
26. Wang, T. H.; Fang, T.-H.; Kang, S.-H.; Lin, Y.-C. Nanoindentation Characteristics of Clamped Cu Membranes. *Nanotechnology* **2007**, 135701(1–6).
27. Lee, C.; Wei, X.; Kysar, J. W.; Hone, J. W. Measurement of the Elastic Properties and Intrinsic Strength of Monolayer Graphene. *Science* **2008**, *321*, 385–388.
28. Page, T. F.; Hainsworth, S. V. Using Nanoindentation Techniques for the Characterization of Coated Systems: A Critique. *Surf. Coat. Technol.* **1993**, *61*, 201–208.
29. Ramsey, P. M.; Chandler, H. W.; Page, T. F. Modelling the Contact Response of Coated Systems. *Surf. Coat. Technol.* **1991**, *49*, 504–509.
30. McGurk, M. R.; Chandler, H. W.; Twigg, P. C.; Page, T. F. Modelling the Hardness Response of Coated Systems: The Plate Bending Approach. *Surf. Coat. Technol.* **1994**, *68–69*, 576–581.
31. Gerberich, W. W.; Strojny, A.; Yoder, K.; Cheng, L. Hard Protective Overlayers on Viscoelastic-Plastic Substrates. *J. Mater. Res.* **1999**, *14*, 2210–2218.
32. Yoo, Y.; Lee, W.; Shin, H. Spherical Nano-indentation of a Hard Thin-Film/Soft Substrate Layered System: I. Critical Indentation Depth. *Modelling Simul. Mater. Sci. Eng.* **2004**, *12*, 59–67.
33. Yoo, Y.; Lee, W.; Shin, H. Spherical Nano-indentation of a Hard Thin-Film/Soft Substrate Layered System: II. Evolution of Stress and Strain Fields. *Modelling Simul. Mater. Sci. Eng.* **2004**, *12*, 69–78.
34. Johnson, L. K. *Contact Mechanics*; Cambridge University Press: New York, 1985.
35. Carpick, R. W.; Ogletree, D. F.; Salmeron, M. Lateral Stiffness: A New Nanomechanical Measurement for the Determination of Shear Strengths with Friction Force Microscopy. *Appl. Phys. Lett.* **1997**, *70*, 1548–1550.
36. Janmey, P. A.; McCulloch, C. A. Cell Mechanics: Integrating Cell Response to Mechanical Stimuli. *Annu. Rev. Biomed. Eng.* **2007**, *9*, 1–34.
37. Duffy, D. C.; McDonald, J. C.; Schueller, O. J. A.; Whitesides, G. M. Rapid Prototyping of Microfluidic Systems in Poly(dimethylsiloxane). *Anal. Chem.* **1998**, *70*, 4974–4984.
38. Villarrubia, J. S. Algorithms for Scanned Probe Microscope, Image Simulation, Surface Reconstruction, and Tip Estimation. *J. Res. Natl. Inst. Stand. Technol.* **1997**, *102*, 435–454.